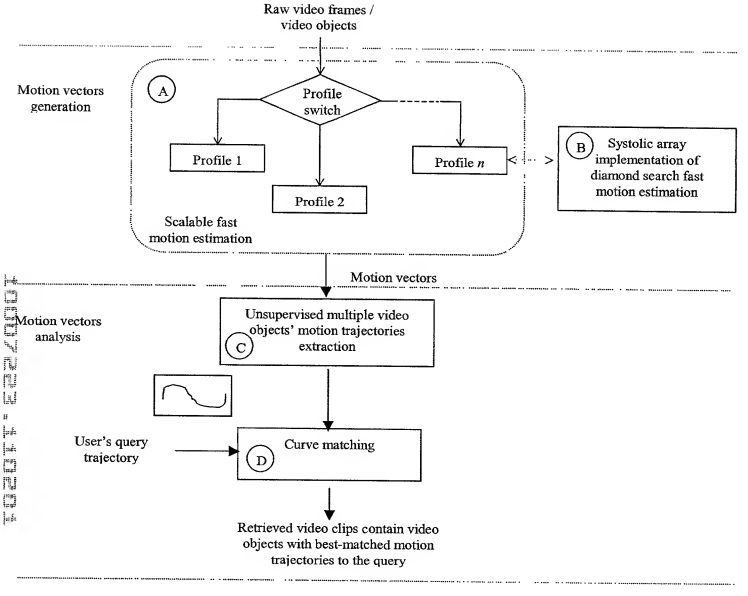
Raw video frames / video objects
Motion vectors generation
A
Profile switch
Profile 1
Profile 2
Profile n
B
Systolic array implementation of diamond search fast motion estimation
Scalable fast motion estimation
Motion vectors
Motion vectors analysis
Unsupervised multiple video objects' motion trajectories extraction
C
User's query trajectory
Curve matching
D
Retrieved video clips contain video objects with best-matched motion trajectories to the query

Figure 1

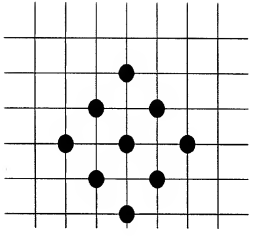

Fig. 2(a) Large Diamond Search Pattern (LDSP)

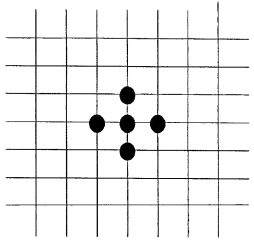

Fig. 2 (b) Small Diamond Search Pattern (SDSP)

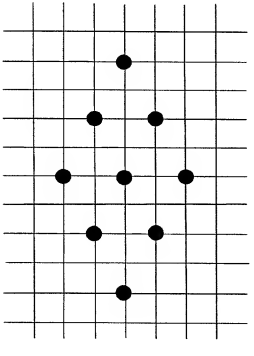

Fig. 3(a) Large Diamond Search Pat. (LDSP)

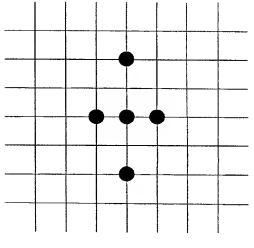

Fig. 3(b) Small Diamond Search Pat.(SDSP)

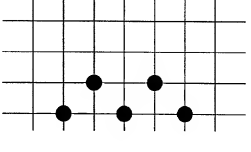

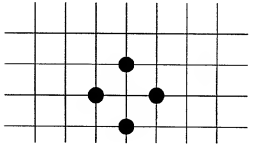

FIG.4 (a) Horizontal Hexagon Search Pattern (HHSP)

Fig. 4(b) Vertical Hexagon Search Pattern (VHSP)

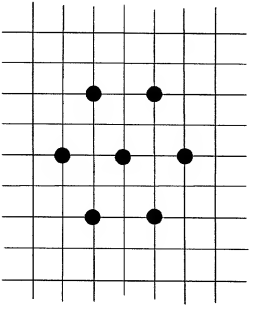

Fig. 4(c) Interlaced Hexagon Search Pattern (IHSP)

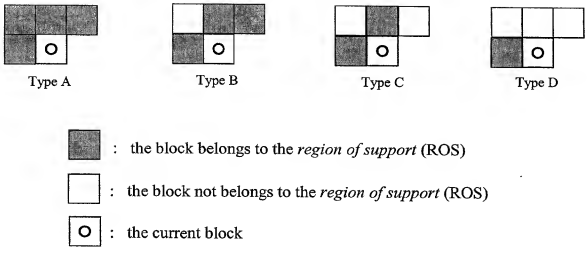

Figure 5: Various types of *region of support* (ROS)

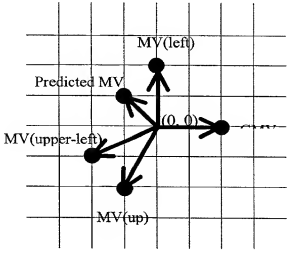

Fig. 6(a). Motion Adaptive Pattern (MAP)

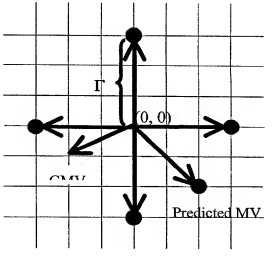

Fig. 6(b). Adaptive Rood Pattern (ARP)

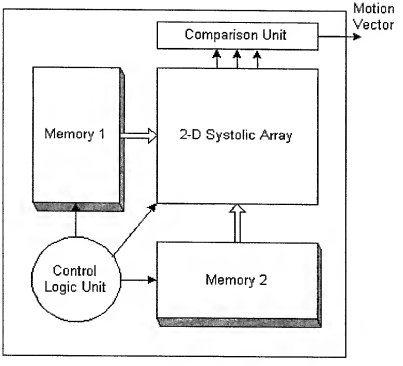

Fig. 7. A system architecture for a 2-D systolic array

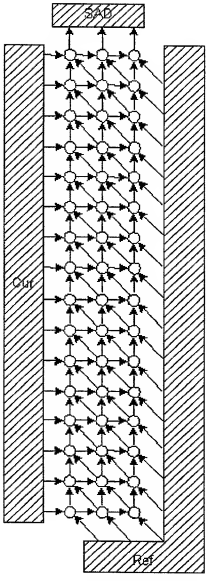

Fig. 8. An illustration of a systolic array organization

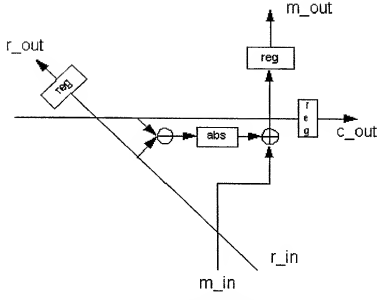

Fig. 9. A typical *processing element* (PE) structure

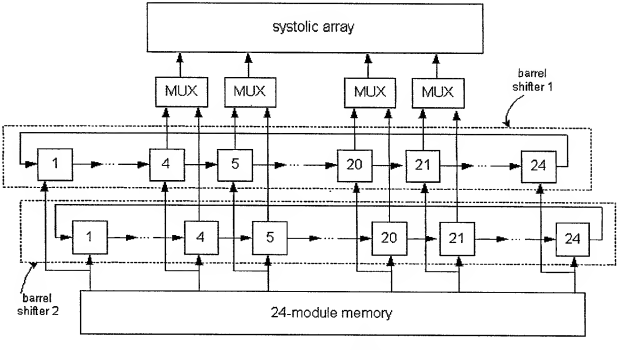

Fig. 10. An illustration of barrel shifter architecture

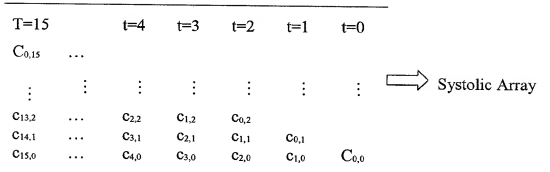

Fig. 11(a) Current-block data

Systolic Array

	t=0	$r_{0,0}$	$r_{0,1}$	$r_{0,2}$	$r_{0,3}$	...	...	$r_{0,15}$	*	*
	t=1	$r_{1,0}$	$r_{1,1}$	$r_{1,2}$	$r_{1,3}$	...	...	$r_{1,15}$	$r_{1,16}$	*
	t=2	$r_{2,0}$	$r_{2,1}$	$r_{2,2}$	$r_{2,3}$	...	...	$r_{2,15}$	$r_{2,16}$	$r_{2,17}$
	⋮	⋮	⋮	⋮	⋮	⋮	⋮	⋮	⋮	⋮
	t=15	$r_{15,0}$	$r_{15,1}$	$r_{15,2}$	$r_{15,3}$	...	...	$r_{15,15}$	$r_{15,16}$	$r_{15,17}$
slot 1	t=16	*	$r_{16,1}$	$r_{16,2}$	$r_{16,3}$	...	...	$r_{16,15}$	$r_{16,16}$	$r_{16,17}$
slot 2	t=17	*	*	$r_{17,2}$	$r_{17,3}$	...	...	$r_{17,15}$	$r_{17,16}$	$r_{17,17}$
	t=18	$r_{1,-1}$	$r_{1,0}$	$r_{1,1}$	$r_{1,2}$	...	...	$r_{1,14}$	*	*
	t=19	$r_{2,-1}$	$r_{2,0}$	$r_{2,1}$	$r_{2,2}$	...	...	$r_{2,14}$	$r_{2,15}$	*
	t=20	$r_{3,-1}$	$r_{3,0}$	$r_{3,1}$	$r_{3,2}$	...	...	$r_{3,14}$	$r_{3,15}$	$r_{3,16}$
	⋮	⋮	⋮	⋮	⋮	⋮	⋮	⋮	⋮	⋮
	t=33	$r_{16,-1}$	$r_{16,0}$	$r_{16,1}$	$r_{16,2}$	...	...	$r_{16,14}$	$r_{16,15}$	$r_{16,16}$
slot 1	t=34	*	$r_{17,0}$	$r_{17,1}$	$r_{17,2}$	...	...	$r_{17,14}$	$r_{17,15}$	$r_{17,16}$
slot 2	t=35	*	*	$r_{18,1}$	$r_{18,2}$	...	...	$r_{18,14}$	$r_{18,15}$	$r_{18,16}$
	t=36	$r_{2,-2}$	$r_{2,-1}$	$r_{2,0}$	$r_{2,1}$	...	...	$r_{2,13}$	*	*
	t=37	$r_{3,-2}$	$r_{3,-1}$	$r_{3,0}$	$r_{3,1}$	...	...	$r_{3,13}$	$r_{3,14}$	*
	⋮	⋮	⋮	⋮	⋮	⋮	⋮	⋮	⋮	⋮

Fig. 11(b) Reference-block data

Fig. 11. Time scheduling of data: (a) Current-block data and (b) Reference-block data

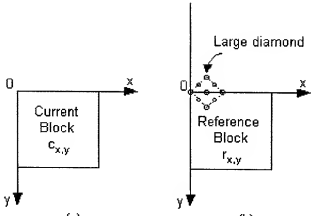

Fig. 12: The actual subscript positions with respect to the positions in: (a) the current and (b) reference images.

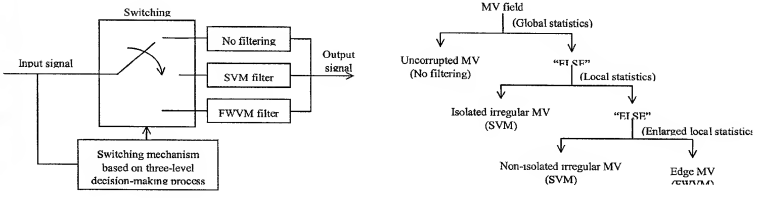

Figure 13: (a) The architecture of the switching-based median filter; (b) The hierarchical decision-making process for identifying each MV's characteristic and the corresponding filtering action taken.

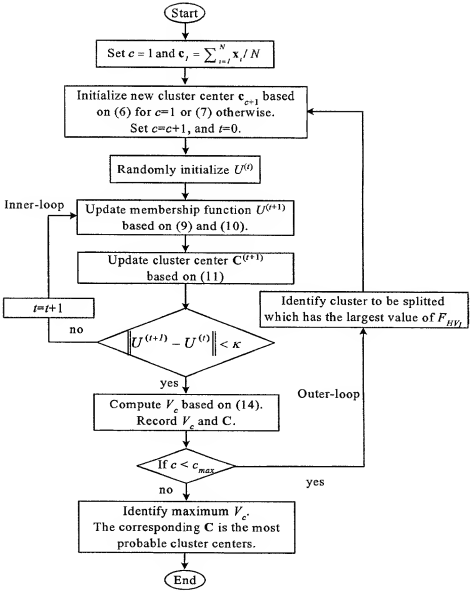

Figure 14: The architecture of the *maximum entropy fuzzy clustering* (MEFC) to achieve unsupervised identification of clusters without any *a priori* assumption.

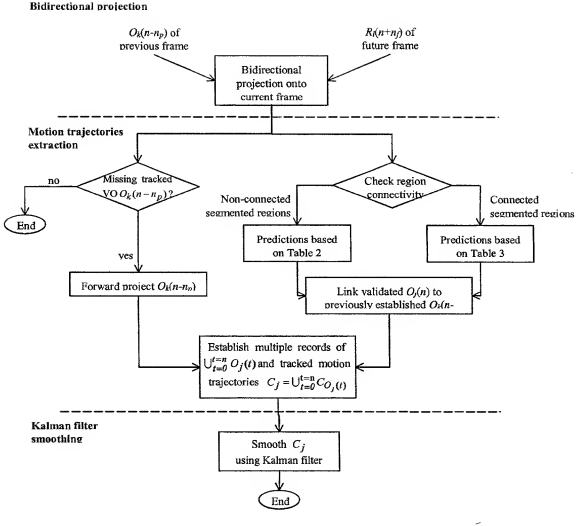

Figure 15: Three main stages of the bidirectional motion tracking scheme, comprising bi-directional projection, recursive VO tracking and validating, as well as Kalman filter smoothing.